Journal of Metals, Materials and Minerals, Vol. 32, No. 1, pp. 124-133, 2022

Synthesis and phosphate adsorption performance of elephant dung biochar modified with magnesium and iron

Navod ABEYSINGHE[1], Kaewta JETSRISUPARB[2,3], K.H.T. KARUNARATHNA[4], E.P.S. CHANDANA[4], Siraprapa SUWANREE[2], Pornnapa KASEMSIRI[2,3], Prinya CHINDAPRASIRT[3,5], and Jesper T.N. KNIJNENBURG[1,3,*]

[1] *International College, Khon Kaen University, Khon Kaen, 40002, Thailand*
[2] *Department of Chemical Engineering, Khon Kaen University, Khon Kaen, 40002, Thailand*
[3] *Sustainable Infrastructure Research and Development Center, Khon Kaen University, Khon Kaen, 40002, Thailand*
[4] *Department of Biosystems Technology, Faculty of Technology, University of Ruhuna, Matara, 81000, Sri Lanka*
[5] *Department of Civil Engineering, Khon Kaen University, Khon Kaen, 40002, Thailand*

***Corresponding author e-mail:** jespth@kku.ac.th

Received date:
7 September 2021
Revised date
6 October 2021
Accepted date:
16 November 2021

Keywords:
Adsorption;
Biochar;
Elephant dung;
Phosphate;
Pyrolysis

Abstract

The large production volume combined with the high lignocellulose content makes elephant dung an attractive and underutilized biomass resource, but also presents waste management problems for elephant orphanages. This study explored the conversion of elephant dung into biochars by slow pyrolysis at 500°C for the recovery of phosphate. The unmodified biochar (BC500) had a specific surface area (S_{BET}) of 62.5 $m^2 \cdot g^{-1}$ with point of zero charge (pH_{PZC}) of 7.7. Biochar modification with $MgCl_2$ (MgBC500) and $FeCl_3$ (FeBC500) by pre-pyrolysis treatment affected the S_{BET} (48.7 $m^2 \cdot g^{-1}$ and 259.4 $m^2 \cdot g^{-1}$, respectively) and pH_{PZC} (8.7 and 3.3, respectively). In FeBC500, Fe was present as magnetite (Fe_3O_4) and hematite (α-Fe_2O_3) as confirmed by X-ray diffraction. Instead of adsorption, both BC500 and MgBC500 released phosphate at pH 3-6. Phosphate adsorption onto FeBC500 reached equilibrium within 24 h and followed pseudo-second order kinetics. The adsorption isotherm was best described with the Langmuir equation with a maximum adsorption capacity of 0.744 mg-P·g^{-1}. The phosphate adsorption behavior was related to the pH_{PZC} and metal content of the biochar. Conversion of elephant dung into biochar presents an environmentally friendly waste management solution that may find further applications in the adsorption of other nutrients or pollutants.

1. Introduction

The Asian elephant (*Elephas maximus*) is the largest living land animal in Asia and is distributed throughout Southeast Asia and the Indian subcontinent. The diet of an elephant consists of 30% to 50% woody biomass [1] and an adult elephant can produce up to 150 kg dung per day [2]. Due to the mere volumes being produced, the disposal of domesticated elephant waste becomes a problem to elephant orphanages. Additionally, elephant dung could present an elevated risk for environmental contamination through the release of pathogens into water and emissions of odor and toxic gases [2,3]. There is thus a need to properly dispose of the large quantities of dung being produced in elephant orphanages.

Elephant dung can be seen as a valuable source of lignocellulosic biomass that contains 34% to 47% cellulose, 19% to 28% hemicellulose and 14% to 18% lignin [3,4], but is still not fully utilized [5]. As value-added products, previous studies have converted elephant dung into a biocoal fuel [2] and methane through anaerobic digestion [3]. The dung of elephants and other animals have also been used for the production of pulp, paper, and composite materials [5].

Biochar is a carbonaceous solid produced by thermochemical conversion (pyrolysis) of organic feedstock in a limited oxygen environment [6]. In the last decades, biochar has received great attention as sorbent for the removal of various pollutants [6] and the recovery of nutrients [7,8]. Application of biochar to soil improves the water holding capacity and nutrient retention, which leads to lower fertilizer requirements and reduced nutrient leaching [9]. Biochars are typically produced from agricultural wastes, but have also been prepared from the manure and dung of various animals (e.g., cow, yak, swine, and poultry) [10-13]. Relatively little research has been done on the preparation of biochar from elephant dung. Suma *et al.* [14,15] pyrolyzed elephant dung at 350°C for 15 min, and the resulting biochar with specific surface area of 5.69 $m^2 \cdot g^{-1}$ was used for the removal of cationic compounds (methylene blue and Fe(III)). Theivarasu and Chandra [16] produced an activated carbon (specific surface area 37.869 $m^2 \cdot g^{-1}$) by treatment of elephant dung with concentrated H_2SO_4 at 120°C for 3 h, which was used for the removal of an anionic dye, Reactive Yellow 15. These studies show that porous carbons produced from elephant dung can be used for the adsorption of both cationic and anionic compounds.

Throughout the past decades, phosphorus (P) fertilizers have been excessively applied in order to satisfy the growing demands for food production. However, only a small fraction of the applied fertilizer is taken up by crops, and the excess P may end up in water systems resulting

in environmental problems like algal blooms and eutrophication. The reduction in available P resources further necessitates the recovery of P from wastewaters [17]. Compared to other sorbents, using biochars to recover phosphate by adsorption has received great attention because of the low cost, environmental friendliness, high porosity, versatility, and tunable properties of biochar. Ideally, P-loaded biochars would then directly be used in the field as P source for crops while simultaneously enhancing soil properties [12]. Unmodified biochars generally have low adsorption capacity for phosphate due to the lack of specific interaction sites [7] and modification of the biochar to incorporate active sites for phosphate adsorption is thus required. Particularly the introduction of metals such as Ca, Mg, Fe, or Al by either pre- or post-pyrolysis treatment greatly enhances the biochar properties, as the presence of these elements plays a key role in phosphate capture from water resources [7,8,18].

In this study, elephant dung was converted into a biochar by pyrolysis at 500°C for 2 h. The biochar was loaded with Mg and Fe via pre-pyrolysis treatment of the elephant dung with respectively $MgCl_2$ and $FeCl_3$. The biochars were physicochemically characterized and the phosphate adsorption performance of the Mg- and Fe-treated as well as untreated biochar was evaluated in batch adsorption studies. Based on the literature review, our hypothesis was that modification of elephant dung biochar with Mg and Fe increases the phosphate adsorption capacity of the biochar. To the best of our knowledge, this is the first study that presents the use of biochars derived from elephant dung for the recovery of phosphate.

2. Experimental

2.1 Synthesis of elephant dung biochars

Fresh elephant dung was collected from a healthy 16-year old male Asian elephant at the Pinnawala Elephant Orphanage in Rambukkana, Sri Lanka. This elephant has a daily food intake of approximately 250 kg that consists primarily of fishtail palm trunk and leaves, as well as leaves of jack, coconut, and other trees. The dung was soaked in water to remove the non-fibrous parts, followed by three times washing with tap water and oven drying at 105°C until constant weight. The dried elephant dung fibers were crushed and sieved to maintain homogeneity of the material. Pyrolysis of the elephant dung was carried out at 500°C for 2 h (heating rate 5°C·min^{-1}) in a muffle furnace under low oxygen condition by closing the biomass-filled crucibles. The produced elephant dung biochar (BC500) was stored in a zip lock bag at room temperature. The biochar yield was determined according to Equation (1):

$$Yield = \frac{m_{BC}}{m_i} \times 100\% \quad (1)$$

Here, m_{BC} (g) is the residual biochar mass after pyrolysis, and m_i (g) is the initial mass of the elephant dung before pyrolysis. The Mg- and Fe-modified biochars were prepared following the method used by Zheng *et al*. [18] with slight modifications. Here, 25 g dried elephant dung was soaked in 500 mL of a 200 mM solution of $MgCl_2 \cdot 6H_2O$ (>99%, Honeywell, India) or $FeCl_3$ (anhydrous, 98%, Sisco Research Laboratories Pvt. Ltd., India), respectively. The suspension was kept stirring for 1 h followed by filtration and oven drying at 80°C for 3 h. Pyrolysis was subsequently carried out for 2 h at 500°C as described for the non-modified biochar. The obtained Mg- and Fe-modified biochars were washed five times with distilled water (8 g biochar in 240 mL distilled water) to remove unbound metals until the pH and EC of the water were constant. The washed modified biochars were oven dried at 80°C until constant weight and the product MgBC500 and FeBC500 were stored in zip lock bags at room temperature. The yield of MgBC500 and FeBC500 was determined according to Equation (1), with the initial elephant dung mass m_i as the mass after impregnation with respectively $MgCl_2$ or $FeCl_3$.

2.2 Biochar characterization

The pH and electrical conductivity (EC) of the biochars in deionized (DI) water were measured in triplicate following the recommended procedures of Singh *et al*. [19]. The point of zero charge (pH_{PZC}) of the biochars was determined by solid addition method according to Liu *et al.* [20]. Nitrogen adsorption isotherms (41 points) were measured at 77 K on a Micrometrics ASAP 2460. Before analysis, the samples were dried at 180°C followed by degassing overnight under vacuum at 200°C. The total pore volume (V_T) was estimated from the nitrogen adsorbed at P/Po of approximately 0.99, and the micropore volume (V_{micro}) was determined from the t-plot. The average pore diameter (D_p) was calculated by the BJH method using desorption data. The X-ray diffraction (XRD) patterns were collected using a PANalytical EMPYREAN with Cu Kα radiation (40 kV, 45 mA) over $2\theta = 5°$ to 80°. Phase identification was done using QualX2.0 software (version 2.24) [21]. Fourier Transform Infrared (ATR-FTIR) spectra were collected on a Bruker TENSOR27 in the range 600 cm^{-1} to 4000 cm^{-1} by accumulating 32 scans with resolution 2 cm^{-1} [22]. Scanning electron microscopy (SEM) images were taken on a Hitachi SU3800. The samples were sputter-coated with gold before SEM analysis.

Thermogravimetric analysis was done on a Shimadzu DTG-60H based on the procedure adapted from Crombie *et al.* [23]. Approximately 5 mg of each biochar sample was weighed in a platinum pan and heated to 800°C (heating rate 10 °C·min^{-1}) under 60 mL·min^{-1} N_2 flow. The temperature was kept at 800°C for 20 min, after which the atmosphere was changed to air (60 mL·min^{-1}) for 20 min. The moisture content (MC), volatile matter (VM), fixed carbon (FC) and ash contents were determined from the thermogravimetry data according to Equations (2)-(5):

$$MC = \frac{m_1 - m_2}{m_1} \times 100\% \quad (2)$$

$$VM = \frac{m_2 - m_3}{m_2} \times 100\% \quad (3)$$

$$FC = \frac{m_3 - m_4}{m_2} \times 100\% \quad (4)$$

$$Ash = \frac{m_4}{m_2} \times 100\% \quad (5)$$

Here, m_1 (mg) is the initial sample weight, m_2 (mg) is the dry weight determined at 205°C, m_3 (mg) is the sample weight at 800°C in N_2 atmosphere, and m_4 (mg) is the final sample weight at 800°C after introduction of air. The VM, FC and ash are reported per dry weight (%dw), whereas the moisture content (%) is relative to the fresh material.

The total metal (Ca, Mg, Fe, and K) and P contents of the biochars were measured in triplicate after digestion by modified dry ashing [24]. Concentrations of Ca, Mg, Fe, and K in the digested solutions were measured using flame atomic absorption spectroscopy (Perkin Elmer PinAAcle 900 F) with external calibration after dilution in 1% HNO_3. The P concentration in the filtrate was measured by molybdenum blue method and the absorbance at 880 nm was measured by UV-vis spectrophotometer (Agilent 8453) with external calibration [25].

2.3 Phosphate adsorption studies

All phosphate adsorption experiments were carried out at room temperature, and all solutions were prepared using DI water (18.2 MΩ). Phosphate standard solutions were prepared using KH_2PO_4 (99.5%, RCI Labscan Ltd.). To study the effect of pH on phosphate adsorption, 100 mg of each biochar sample was mixed with 40 mL of a solution containing 10 mg-P·L^{-1}, and the pH was carefully adjusted to 3, 4, 5, or 6 using dilute HCl or NaOH. The suspensions were kept shaking (120 rpm) at room temperature for 24 h, at which point the solutions were filtered through a membrane syringe filter (0.22 μm) and the residual P concentrations were measured by UV-vis spectroscopy as described previously.

The phosphate adsorption kinetics onto FeBC500 were studied by dispersing 500 mg biochar in 200 mL of 10 mg-P·L^{-1}solution. The pH of the phosphate solution was not adjusted and was 4.5 after addition of FeBC500. At each time point, a 2 mL sample was taken, filtered (0.22 μm) and the phosphate concentration was measured by UV-vis spectroscopy as described previously. Adsorption kinetics were modeled in the kinetic region (up to 24 h) using the pseudo-first order model, pseudo-second order model, intraparticle diffusion model, and Elovich model given in respectively Equations (6)-(9):

$$q_t = q_e\left[1-e^{-k_1 t}\right] \tag{6}$$

$$q_t = q_e \frac{k_2 q_e t}{1+k_2 q_e t} \tag{7}$$

$$q_t = k_i \cdot t^{1/2} + C_i \tag{8}$$

$$q_t = \frac{1}{\beta} \ln \alpha\beta + \frac{1}{\beta} \ln t \tag{9}$$

Here, q_t and q_e (mg-P·g^{-1}) are the P adsorbed at time t and at equilibrium, respectively, k_1 (h^{-1}) is the first order rate constant, k_2 (g·mg^{-1}·h^{-1}) is the second order rate constant, k_i (mg·g^{-1}·h$^{-0.5}$) is the intraparticle diffusion rate, C_i (mg·g^{-1}) is a constant that gives information about the boundary layer thickness, α (g·mg^{-1}·h^{-1}) is the initial P adsorption rate, and β (g·mg^{-1}) is the desorption constant. Each function was converted into its linear form and data were fitted by linear regression. The coefficient of determination (R^2) was used to evaluate the suitability of each model to describe the experimental data.

The phosphate adsorption isotherm onto FeBC500 was measured by dispersing 100 mg biochar in 40 mL solutions with different initial P concentrations ranging from 1 to 50 mg-P·L^{-1}. After 24 h, the solutions were filtered (0.22 μm) and the P concentration in the solutions was measured by UV-vis spectroscopy as described previously. The adsorption isotherm was modeled with the Langmuir and Freundlich equations. The Langmuir model assumes that adsorption sites are energetically homogeneous and monolayer adsorption takes place without interaction between adsorbed molecules. The Langmuir isotherm is given by Equation (10):

$$q_e = \frac{K_L q_m C_e}{1+K_L C_e} \tag{10}$$

Here, q_e (mg-P·g^{-1}) is the equilibrium P adsorption capacity, C_e (mg-P·L^{-1}) is the equilibrium P concentration, q_m (mg-P·g^{-1}) is the maximum P adsorption capacity and K_L (L·mg^{-1}) is the Langmuir constant. The favorability of the adsorption process for the Langmuir isotherm was calculated with the separation factor R_L in Equation (11):

$$R_L = \frac{1}{1+K_L C_e} \tag{11}$$

A value of R_L between 0 and 1 means that the adsorption is considered favorable. In contrast to the Langmuir model, the Freundlich model assumes heterogeneous surface sites with a non-uniform distribution of heat of adsorption. The Freundlich equation is given by Equation (12):

$$q_e = K_F C_e^{1/n} \tag{12}$$

Here, K_F ((mg·g^{-1})(L·mg^{-1})$^{1/n}$) is the Freundlich constant and n is the Freundlich exponent. Each isotherm function was converted into its linear form and data were fitted by linear regression. The coefficient of determination (R^2) was used to evaluate the suitability of each model to describe the experimental data.

3. Results and discussion

3.1 General properties of the biochars

Table 1 summarizes selected material properties of the synthesized elephant dung biochars. The yield of the unmodified biochar (BC500) was 35%, which is in good agreement with previous studies [26]. The BC500 had an alkaline pH of 8.4 as is typical for animal manure biochars [10,11], while the EC of 135 μS·cm^{-1} was lower than that of biochars produced from animal manure [10]. The BC500 had a high fixed carbon (FC) content of 51.2% which is much higher than that of animal manure biochars [10], and consequently a lower volatile matter (VM) and ash content.

Modification of the biochar with $MgCl_2$ produced MgBC500, with a lower yield than BC500 but higher pH and EC due to the alkaline character of Mg compounds. The yield for FeBC500 is comparable to that of Mojoudi *et al.* [27]. The lower yield of MgBC500 and FeBC500 compared to BC500 is ascribed to the introduction of $MgCl_2$ and $FeCl_3$, respectively, that facilitated the biomass pyrolysis [28]. The hydrolysis of the incorporated Fe released a high amount of H^+ that reduced the biochar pH to 2.7 [29]. The FeBC500 had the highest ash content of 18.9% and can be ascribed to the retention of Fe-containing compounds in the biochar [29].

Table 1. General properties of the elephant dung biochars BC500, MgBC500, and FeBC500.

Material	Yield (%)	pH (-)	EC (µS·cm^{-1})	MC (%)	VM (% dw)	FC (% dw)	Ash (% dw)
BC500	35.0	8.4	135	8.7	34.7	50.9	14.4
MgBC500	29.3	10.2	362	13.5	39.1	45.5	15.4
FeBC500	33.1	2.7	863	7.7	32.1	49.0	18.9

Table 2. Total concentrations of metals (Ca, Mg, Fe, K) and P in the elephant dung biochars.

Material	Ca (mg·g^{-1})	Mg (mg·g^{-1})	Fe (mg·g^{-1})	K (mg·g^{-1})	P (mg·g^{-1})
BC500	4.0	2.1	2.1	1.1	4.1
MgBC500	2.2	26.1	1.3	0.3	3.3
FeBC500	0.3	0.7	39.0	0.2	3.5

The total metal (Ca, Mg, Fe, and K) and P contents of the biochars are summarized in Table 2. The unmodified BC500 contained comparatively small amounts (1.1 mg·g^{-1} to 4.0 mg·g^{-1}) of Ca, Mg, Fe, and K, in decreasing order, which are lower than biochars produced from yak manure [11] and cow dung [13]. As expected, modification with $MgCl_2$ increased the Mg content to 26.1 mg·g^{-1} in MgBC500, confirming the incorporation of Mg, in agreement with previous work [30]. Similarly, modification with $FeCl_3$ increased the Fe content in FeBC500 to 39.0 mg·g^{-1} [18,31]. When held next to a magnet, FeBC500 was found to possess magnetic properties. All three biochars contained a small amount of P between 3.3 mg·g^{-1} to 4.1 mg·g^{-1}.

3.2 Biochar morphology and pore structure

Figure 1 shows typical SEM images of the biochars at 1000x magnification. All three biochars exhibited a porous structure [15] that originated from the fibrous residue in the elephant dung. No clear effect of Mg modification on the morphology of MgBC500 was visible. Modification with Fe in FeBC500, on the other hand, increased the surface roughness that may be due to the deposition of Fe oxides [32].

Table 3 summarizes the surface area and porous properties obtained from the nitrogen adsorption measurements. Without modifier, BC500 had an S_{BET} of 62.5 m^2·g^{-1} that is typical for biochars produced under similar conditions [26]. The total pore volume V_T of BC500 was 0.056 cm^3·g^{-1}, of which 44% was microporous, and the average pore diameter D_p was 19.3 nm. Upon incorporation of Mg, the S_{BET} of MgBC500 decreased to 48.7 m^2·g^{-1} and D_p was reduced to 8.9 nm, which was likely due to blockage of pores [30]. In contrast to MgBC500, biochar modification with Fe greatly increased the S_{BET} by a factor of four to 259.4 m^2·g^{-1} for FeBC500. The fourfold increase in V_{micro} and the reduction in D_P further confirmed that $FeCl_3$ promoted the formation of micropores [33,34].

3.3 X-ray diffraction patterns

The XRD patterns of the biochars are shown in Figure 2. The unmodified biochar BC500 was largely amorphous showing a broad diffraction hump around 2θ = 25° and a smaller hump at 43° due to carbon [34]. A small peak at 2θ = 29.4° was found that may be indicative of diopside ($CaMgSi_2O_6$). Upon incorporation of Mg there was no strong change in the crystallinity, and the XRD pattern of MgBC500 is very similar to that of BC500. No crystalline Mg-containing phase was observed, likely due to the low Mg content in the biochar.

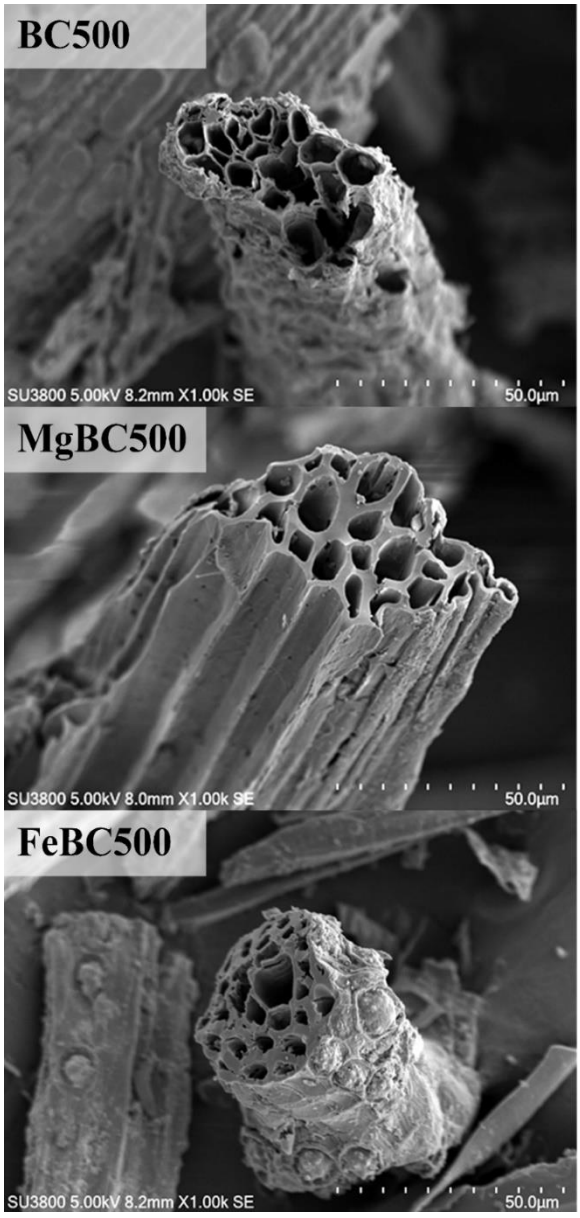

Figure 1. Scanning electron microscopy images of the elephant dung biochars

Table 3. BET specific surface area (S_{BET}), total pore volume (V_T), micropore volume (V_{micro}), and average pore diameter (D_p) of the elephant dung biochars. Values in brackets indicate the percentage contribution of V_{micro} to V_T.

Material	S_{BET} ($m^2 \cdot g^{-1}$)	V_T ($cm^3 \cdot g^{-1}$)	V_{micro} ($cm^3 \cdot g^{-1}$)	D_p (nm)
BC500	62.5	0.056	0.025 (44%)	19.3
MgBC500	48.7	0.040	0.018 (44%)	8.9
FeBC500	259.4	0.141	0.102 (72%)	3.4

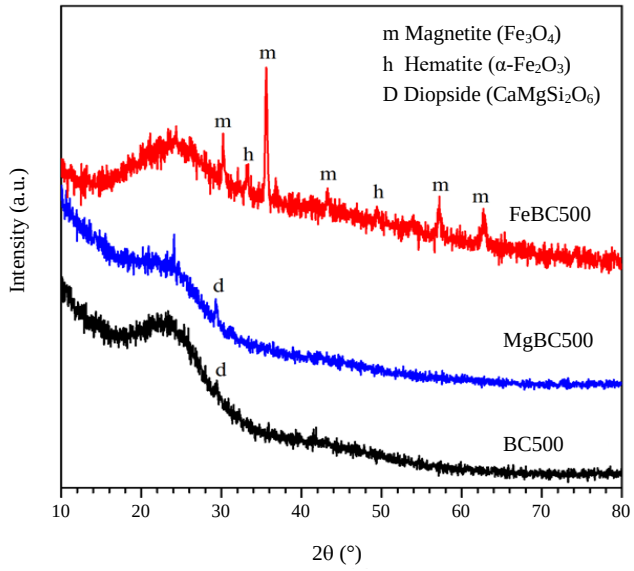

Figure 2. X-ray diffraction patterns of BC500, MgBC500, and FeBC500. The following ICDD cards were used for phase identification: magnetite (88-0866), hematite (89-0597), and diopside (78-1390).

The Fe-modified biochar FeBC500 contained peaks of magnetite (Fe_3O_4) and a small fraction of hematite (α-Fe_2O_3). Magnetite is commonly observed in $FeCl_3$-treated biochars, sometimes in co-existence with α-Fe_2O_3 [33]. Thermal decomposition of $FeCl_3$ resulted in the formation of crystalline α-Fe_2O_3 [35], which was further converted into Fe_3O_4 by reacting with the carbon formed during carbonization [33].

3.4 Fourier transform infrared (FTIR) spectra

Figure 3 displays the FTIR spectra of the biochars. The spectrum for the unmodified biochar (BC500) showed adsorption peaks that are typical for biochars produced from lignocellulosic materials [36]. The main peak at 1075 cm^{-1} originated from C-O stretching and deformation [36]. The peak at 1586 cm^{-1} was indicative of aromatic C=C bonds [36,37], and the shoulder peak at 1694 cm^{-1} may be ascribed to C=O vibrations from carboxylate groups [37]. The peak at 1404 cm^{-1} may correspond to C-H bending or carboxylic O-H vibrations [36]. The aromatic C-H stretching vibrations are visible at 785 cm^{-1}, whereas the peak at 692 cm^{-1} was ascribed to C-C stretching vibrations [36]. The broad band at 3232 cm^{-1} was due to O-H stretching vibrations in hydroxyl groups [36]. The sharp peak at 877 cm^{-1} may indicate the presence of an inorganic carbonate or is sometimes ascribed to oxygen-substituted aromatic compounds [38].

In the FTIR spectrum of MgBC500, the aromatic C=C peak at 1569 cm^{-1} has increased in intensity, suggesting a more aromatic structure compared to BC500 [30]. This coincides with a relative decrease in the C-O peak intensity at 1031 cm^{-1}. The peak at 1383 cm^{-1} is ascribed to aromatic O-H groups [10], and compared to BC500 the peak intensity at 3208 cm^{-1} has increased, which may suggest an increase in O-H groups on the surface [39]. In the case of FeBC500, the shoulder peak at 1697 cm^{-1} (C=O stretching vibrations in carboxylic acid groups) has sharpened and increased in intensity, demonstrating an increase in carboxylic acid groups content upon pre-treatment with $FeCl_3$. Moreover, the increase in peak intensity at 1583 cm^{-1} compared to BC500 indicated an increase in aromatic C=C content due to aromatization [34,37], but this effect was less than compared to MgBC500.

3.5 Point of zero charge

The pH at the point of zero charge (pH_{PZC}) of the biochars was measured to study the suitability of the biochars for the removal of phosphate. At a solution pH below pH_{PZC}, the surface of the biochar has a net positive charge, which is favorable for the removal of negatively charged ions such as phosphate. Conversely, if the pH of the solution is higher than the pH_{PZC}, the biochar net surface charge is negative, which would attract cations and repel anions. The pH_{PZC} of BC500, MgBC500, and FeBC500 was 7.7, 8.7, and 3.3, respectively (Figure 4). A slightly alkaline pH_{PZC} is typical for unmodified biochars [20,31]. Modification with $MgCl_2$ resulted in a higher pH_{PZC} due to the incorporation of Mg [18]. The low pH_{PZC} of 3.3 for FeBC500 was comparable to previous studies [40].

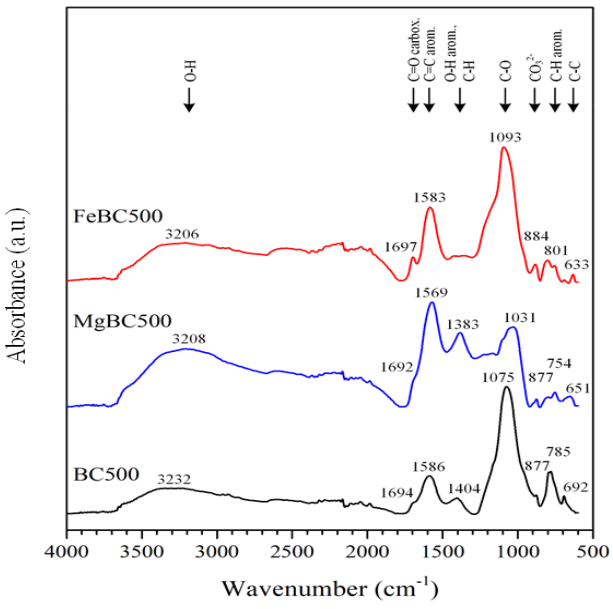

Figure 3. FTIR spectra of BC500, MgBC500, and FeBC500. Numbers above each peak indicate the positions of the major peaks and arrows indicate the corresponding bonds.

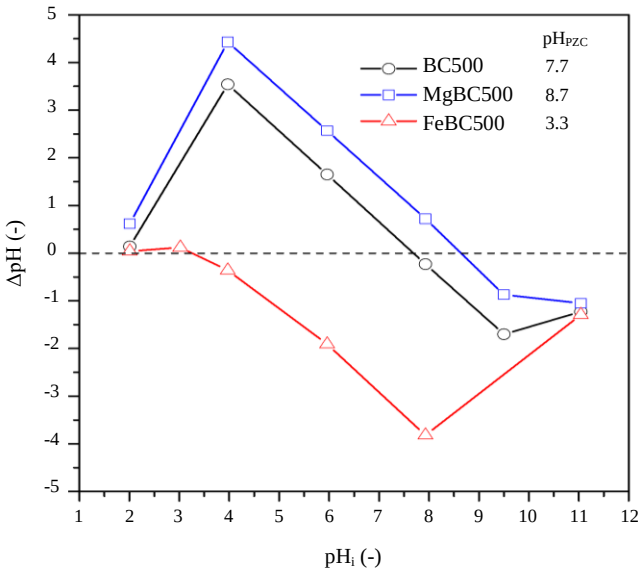

Figure 4. Determination of the point of zero charge (pH_{PZC}) of BC500, MgBC500, and FeBC500.

3.6 Phosphate adsorption onto elephant dung biochars

Phosphate adsorption onto BC500, MgBC500, and FeBC500 was studied in 10 mg-P·L^{-1} solutions with pH adjusted to 3-6 (Figure 5). This pH range was selected based on the phosphate species existing at these conditions. In aqueous solutions, phosphates can exist in four different species (H_3PO_4, $H_2PO_4^-$, HPO_4^{2-}, and PO_4^{3-}), depending on the solution pH:

$$H_3PO_4 \overset{pK_1}{\Leftrightarrow} H_2PO_4^- + H^+ \overset{pK_2}{\Leftrightarrow} HPO_4^{2-} + 2H^+ \overset{pK_3}{\Leftrightarrow} PO_4^{3-} + 3H^+ \quad (13)$$

Here, $pK_1 = 2.13$, $pK_2 = 7.20$, and $pK_3 = 12.33$ [7]. The $H_2PO_4^-$ form, which is the dominant species at pH 3-6, is generally easier adsorbed onto metal oxides than HPO_4^{2-} [31].

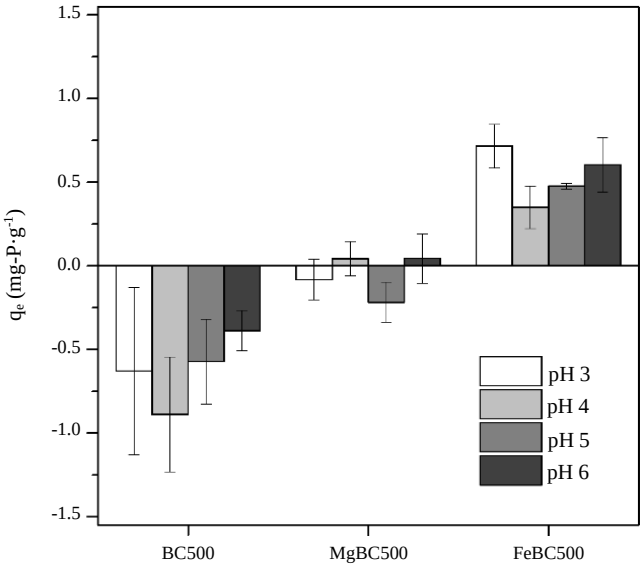

Figure 5. Phosphate adsorption onto BC500, MgBC500 and FeBC500 at different initial pH values of 3-6.

The phosphate adsorption by BC500 was negative at pH 3-6, indicating a net phosphate release from the biochar. Previous studies have also seen the release of phosphate from biochars instead of adsorption [28,41]. Likely, the acidic conditions promoted extraction of phosphate from the biochar that resulted in a higher phosphate release than adsorption. The MgBC500 also displayed a negative or neutral phosphate adsorption but less negative than BC500. This may indicate that the phosphate released from MgBC500 was largely canceled out by the phosphate that adsorbed onto the biochar, or possibly the incorporation of Mg may have reduced the phosphate release. The FeBC500 showed a positive phosphate adsorption capacity of 0.35-0.72 mg-P·g^{-1}, but there was no clear dependence on the pH. Because of the negative phosphate adsorption of BC500 and MgBC500, the adsorption kinetics and isotherm of phosphate onto FeBC500 were investigated in more detail.

The phosphate adsorption kinetics onto FeBC500 were measured at pH 4.5 and initial concentration of 10 mg-P·L^{-1} (Figure 6). Phosphate adsorption rapidly increased within the first 6 h and then slowly leveled off, and equilibrium was reached within 24 h.

The adsorption kinetics were modeled in the kinetic region up to 24 h using the pseudo-first order model (Equation (6)), pseudo-second order model (Equation (7)), intraparticle diffusion model (Equation (8)), and Elovich model (Equation (9)). Frequently, the intraparticle diffusion model presents multilinearity due to the occurrence of two or more steps in the adsorption process. Here, two regions were identified: in the first region (<0.5 h) a very fast uptake was observed, which was followed by a second region (0.5 h to 24 h) where slower phosphate adsorption took place. The kinetic model parameters and their R^2 values are summarized in Table 4. The pseudo-second order equation ($R^2 = 0.978$) provided a better fit than the pseudo-first order model ($R^2 = 0.920$), the two-stage intraparticle diffusion model ($R^2 = 0.870$), and the Elovich equation ($R^2 = 0.847$). The pseudo-second order model predicted an equilibrium adsorption capacity (q_e) of 0.707 mg-P·g^{-1}, which is in close agreement with the experimental data ($q_{e,exp} = 0.684$ mg-P·g^{-1}). Previous studies on phosphate adsorption on various biochars also found that the pseudo-second order best described the adsorption kinetics [7,27,28].

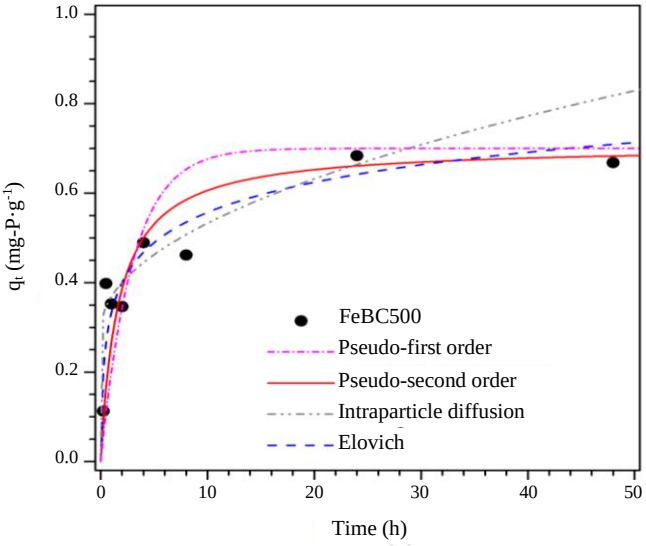

Figure 6. Phosphate adsorption kinetics onto FeBC500.

Table 4. Model parameters and the coefficients of determination (R^2) for phosphate adsorption kinetics onto FeBC500 in the kinetic region (0-24 h). For the intraparticle diffusion model, the parameters are given for the second stage in the two-stage intraparticle diffusion process (t ≥ 0.5 h).

Kinetic model	Parameter 1	Parameter 2	R^2
Pseudo-first order	k_1 = 0.338 h^{-1}	q_e = 0.700 mg-P·g^{-1}	0.920
Pseudo-second order	k_2 = 0.853 g·mg^{-1}·h^{-1}	q_e = 0.707 mg-P·g^{-1}	0.978
Intraparticle diffusion	k_i = 0.076 mg·g^{-1}·$h^{-0.5}$	C_i = 0.293 mg·g^{-1}	0.870
Elovich	α = 319.5 mg·g^{-1}·h^{-1}	β = 0.097 g·mg^{-1}	0.801

Table 5. Langmuir and Freundlich isotherm parameters for the adsorption of phosphate onto FeBC500.

Isotherm model	Parameter 1	Parameter 2	R^2
Langmuir	K_L = 0.150 L·mg^{-1}	q_m = 0.744 mg-P·g^{-1}	0.978
Freundlich	K_F = 0.138 (mg·g^{-1})(L·mg^{-1})$^{1/n}$	n = 2.25	0.922

Generally, adsorption of phosphate onto biochars is governed by electrostatic interactions between the positively charged biochar surface and negatively charged phosphate ions [7]. Here, the pH_{PZC} of FeBC500 was 3.3, which means at the phosphate solution pH of 4.5 the biochar surface had a net negative charge. Phosphate adsorption onto biochar at pH > pH_{PZC}, even though electrostatic interactions are unfavorable, has been observed previously [40,42] and was ascribed to occur via ligand exchange between surface hydroxyl and phosphate anions, forming an inner sphere complex at the sorbent surface [40, 42,43]. Thus apart from electrostatic interactions, other adsorption mechanisms may also be involved. Additionally, while the net biochar surface had a negative charge, the incorporated iron oxides (Fe_3O_4 and α-Fe_2O_3) in FeBC500 may be positively charged at pH 4.5, because the pH_{PZC} of Fe_3O_4 and α-Fe_2O_3 lies between 5 and 8 [44]. In acidic conditions, phosphate is adsorbed onto Fe_3O_4 and α-Fe_2O_3 as the monoprotonated species in either monodentate or bidentate inner sphere complex [40,45]. Thus, it may seem reasonable to assume that phosphate adsorption took place via ligand exchange mechanism onto the Fe_3O_4 and α-Fe_2O_3 present in FeBC500 [40]. The exact mechanism, however, could not be elucidated in the current study.

The influence of the initial phosphate concentration on the adsorption behavior was investigated at initial phosphate concentrations of 1-50 mg-P·L^{-1} at pH 4.5 (Figure 7). The Langmuir (Equation (10)) and Freundlich equations (Equation (12)) were used to describe the phosphate adsorption isotherm onto FeBC500, and a comparison of the two isotherms is given in Table 5. The Langmuir equation provided a better fit (R^2 = 0.978) than the Freundlich equation (R^2 = 0.922), indicating the homogeneous nature of the adsorption sites on the biochar and monolayer adsorption process. The separation factors R_L ranged from 0.12 to 0.91, which indicates that phosphate adsorption onto FeBC500 was favorable. According to the Langmuir equation, the maximum phosphate adsorption capacity of FeBC500 was q_m = 0.744 mg-P·g^{-1}. Generally the maximum phosphate adsorption capacity for Fe-loaded biochars prepared by pre-pyrolysis treatment of the biomass with a Fe source lies between 0.5 and 5 mg-P·g^{-1} [40,43,46], but also higher values have been reported [18,27,31].

Previous studies have identified that important parameters to obtain a high phosphate adsorption capacity are the elemental composition (presence of elements such as Ca, Mg, and Fe) and the surface charge (i.e., pH_{PZC}), and to a lesser extent the specific surface area [7,8]. This may explain the relatively low phosphate adsorption capacity of FeBC500 found here, namely the comparatively low content of Ca (0.3 mg·g^{-1}), Mg (0.7 mg·g^{-1}), and Fe (39.0 mg·g^{-1}) (Table 1) and the low pH_{PZC} of 3.3, despite having a relatively high S_{BET} of 259.4 m^2·g^{-1}. A magnetic biochar derived from water hyacinth had an S_{BET} of only 37.2 m^2·g^{-1} but a very high Fe content of 62.93 wt%, which may explain its adsorption capacity of 5.07 mg-P·g^{-1} [43]. In contrast, a magnetic biochar from corn stalk containing 17.4 wt% Fe with high S_{BET} of 303.1 m^2·g^{-1} and pH_{PZC} of 7.64 had a lower phosphate adsorption capacity of 4.07 mg-P/g [46]. The Fe-loaded rice straw biochars prepared by Wu *et al.* [31] contained only 2.5 wt% to 2.6 wt% Fe, but the high pH_{PZC} of 9.8 to 10.7 as well as the high surface area of 274.4 m^2·g^{-1} to 281.7 m^2·g^{-1} likely contributed to the high phosphate adsorption capacity of >30 mg·g^{-1}. In addition to above properties (metal content, pH_{PZC} and S_{BET}), other factors such as the pH of the solution as well as biomass-specific properties affect the phosphate adsorption performance.

A major challenge that needs to be overcome for the here presented elephant dung biochars is their low P adsorption capacity, which could be enhanced by increasing the Fe and Mg loadings of the biochars. An alternative approach to increase the P content is by co-pyrolysis of the elephant dung with an inexpensive P source: previous studies

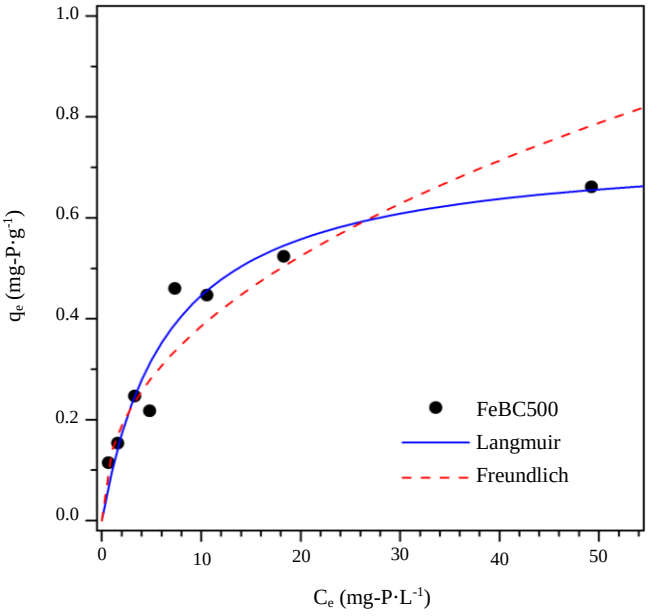

Figure 7. Phosphate adsorption isotherm onto FeBC500.

have demonstrated that such P-loaded biochars can act as slow release fertilizers that effectively supply P to crops [47]. Alternatively, the low pH_{PZC} of 3.3 of FeBC500 means that FeBC500 is negatively charged over a wide pH range, which is beneficial for the adsorption of ammonium [8] or cationic pollutants such as heavy metals like Pb(II) or Cd(II) [48]. This will be further studied in our future work.

4. Conclusions

To the best of our knowledge, this is the first study that examined the use of elephant dung biochar for the recovery of phosphate. Instead of adsorbing phosphate, the unmodified biochar BC500 released phosphate at pH 3-6. While modification of the microporous biochar with Mg greatly increased the Mg content and raised the pH_{PZC} to 8.7, this MgBC500 did not show ability to adsorb phosphate. Modification with Fe, on the other hand, increased the S_{BET} by fourfold and greatly increased the Fe content but resulted in an acidic pH_{PZC} of 3.3. Compared to the other two biochars, FeBC500 adsorbed phosphate with a maximum adsorption capacity of 0.744 mg-P·g^{-1} at pH 4.5. The adsorption behavior can be explained by the low pH_{PZC} and relatively low metal content of the biochar. Adsorption equilibrium was reached after 24 h and adsorption kinetics were best described by pseudo-second order model. Despite the low phosphate adsorption capacity, elephant dung biochar presents an attractive value-added material that may find use for the adsorption of other nutrients and pollutants as well as additive to improve soil properties.

Acknowledgements

The authors would like to acknowledge the “Support by Research and Graduate Studies” Khon Kaen University. Author N.A. kindly acknowledges the Thailand International Postgraduate Programme (TIPP) 2019 scholarship from the Thailand International Cooperation Agency (TICA). The authors would like to thank Miss Wimonporn Iamamornphan for her assistance with the AAS measurements, and Miss Thanawan Jeejaila and Mr. Chanon Saengthip for their assistance with the phosphate measurements by UV-vis spectroscopy.

References

[1] E. Chaudhary, P. Jouquet, C. Rumpel, and R. Sukumar, "Chemical parameters of decomposing dung in tropical forest as indicators of feeding behaviour of large herbivores: A step beyond classical stoichiometry," *Ecological Indicators*, vol. 115, pp. 106407, 2020.

[2] P. Stępień, K. Świechowski, M. Hnat, S. Kugler, S. Stegenta-Dąbrowska, J. A. Koziel, P. Manczarski, and A. Białowiec, "Waste to carbon: Biocoal from elephant dung as new cooking fuel," *Energies*, vol. 12, pp. 4344, 2019.

[3] C. Sawatdeenarunat, S. Saipa, and P. Suaisom, "Anaerobic digestion of elephant camp–derived wastes: methane potential, kinetic study, and biorefinery platform," *Biomass Conversion and Biorefinery*, 2021.

[4] A. F. Saripan and A. Reungsang, "Simultaneous saccharification and fermentation of cellulose for bio-hydrogen production by anaerobic mixed cultures in elephant dung," *International Journal of Hydrogen Energy*, vol. 39, pp. 9028-9035, 2014.

[5] V. Fasake and K. Dashora, "A sustainable potential source of ruminant animal waste material (dung fiber) for various industrial applications: A review," *Bioresource Technology Reports*, vol. 15, pp. 100693, 2021.

[6] J. Wang and S. Wang, "Preparation, modification and environmental application of biochar: A review," *Journal of Cleaner Production*, vol. 227, pp. 1002-1022, 2019.

[7] I. W. Almanassra, G. McKay, V. Kochkodan, M. Ali Atieh, and T. Al-Ansari, "A state of the art review on phosphate removal from water by biochars," *Chemical Engineering Journal*, vol. 409, pp. 128211, 2021.

[8] Q. Yin, B. Zhang, R. Wang, and Z. Zhao, "Biochar as an adsorbent for inorganic nitrogen and phosphorus removal from water: A review," *Environmental Science and Pollution Research*, vol. 24, pp. 26297-26309, 2017.

[9] A. El-Naggar, A. H. El-Naggar, S. M. Shaheen, B. Sarkar, S. X. Chang, D. C. W. Tsang, J. Rinklebe, and Y. S. Ok, "Biochar composition-dependent impacts on soil nutrient release, carbon mineralization, and potential environmental risk: A review," *Journal of Environmental Management*, vol. 241, pp. 458-467, 2019.

[10] K. B. Cantrell, P. G. Hunt, M. Uchimiya, J. M. Novak, and K. S. Ro, "Impact of pyrolysis temperature and manure source on physicochemical characteristics of biochar," *Bioresource Technology*, vol. 107, pp. 419-428, 2012.

[11] J. Zhang, B. Huang, L. Chen, Y. Li, W. Li, and Z. Luo, "Characteristics of biochar produced from yak manure at different pyrolysis temperatures and its effects on the yield and growth of highland barley," *Chemical Speciation and Bioavailability*, vol. 30, pp. 57-67, 2018.

[12] Q. Chen, J. Qin, P. Sun, Z. Cheng, and G. Shen, "Cow dung-derived engineered biochar for reclaiming phosphate from aqueous solution and its validation as slow-release fertilizer in soil-crop system," *Journal of Cleaner Production*, vol. 172, pp. 2009-2018, 2018.

[13] D. Wan, L. Wu, Y. Liu, H. Zhao, J. Fu, and S. Xiao, "Adsorption of low concentration perchlorate from aqueous solution onto modified cow dung biochar: Effective utilization of cow dung, an agricultural waste," *Science of the Total Environment*, vol. 636, pp. 1396-1407, 2018.

[14] Y. Suma, N. Pasukphun, and N. Eaktasang, "Adsorption of methylene blue by low-cost biochar derived from elephant dung," *Applied Environmental Research*, vol. 43, pp. 34-44, 2021.

[15] Y. Suma, N. Pasukphun, and N. Eaktasang, "Efficiency of biochar derived from elephant dung for adsorption of iron (III) ions," *Burapha Science Journal*, vol. 26, pp. 1204-1221, 2021.

[16] C. Theivarasu and S. Chandra, "Adsorption performance of activated carbon prepared from elephant (Elephas maximus) dung for the removal of Reactive Yellow 15 from aqueous solution," *Desalination and Water Treatment*, vol. 51, pp. 7639-7654, 2013.

[17] P. R. Rout, M. K. Shahid, R. R. Dash, P. Bhunia, D. Liu, S. Varjani, T. C. Zhang, and R. Y. Surampalli, "Nutrient

removal from domestic wastewater: A comprehensive review on conventional and advanced technologies," *Journal of Environmental Management*, vol. 296, p. 113246, 2021.

[18] Y. Zheng, A. R. Zimmerman, and B. Gao, "Comparative investigation of characteristics and phosphate removal by engineered biochars with different loadings of magnesium, aluminum, or iron," *Science of the Total Environment*, vol. 747, pp. 141277, 2020.

[19] B. Singh, M. Camps-Arbestain, and J. Lehmann, *Biochar: A guide to analytical methods*. Boca Raton: CRC Press, 2017.

[20] Y. Liu, X. Zhao, J. Li, D. Ma, and R. Han, "Characterization of bio-char from pyrolysis of wheat straw and its evaluation on methylene blue adsorption," *Desalination and Water Treatment*, vol. 46, pp. 115-123, 2012.

[21] A. Altomare, N. Corriero, C. Cuocci, A. Falcicchio, A. Moliterni, and R. Rizzi, "QUALX2.0: A qualitative phase analysis software using the freely available database POW-COD," *Journal of Applied Crystallography*, vol. 48, pp. 598-603, 2015.

[22] J. T. N. Knijnenburg, P. Kasemsiri, K. Amornrantanaworn, S. Suwanree, W. Iamamornphan, P. Chindaprasirt, and K. Jetsrisuparb, "Entrapment of nano-ZnO into alginate/polyvinyl alcohol beads with different crosslinking ions for fertilizer applications," *International Journal of Biological Macromolecules*, vol. 181, pp. 349-356, 2021.

[23] K. Crombie, O. Mašek, S. P. Sohi, P. Brownsort, and A. Cross, "The effect of pyrolysis conditions on biochar stability as determined by three methods," *GCB Bioenergy*, vol. 5, pp. 122-131, 2013.

[24] A. Enders and J. Lehmann, "Comparison of wet-digestion and dry-ashing methods for total elemental analysis of biochar," *Communications in Soil Science and Plant Analysis*, vol. 43, pp. 1042-1052, 2012.

[25] J. T. N. Knijnenburg, K. Laohhasurayotin, P. Khemthong, and W. Kangwansupamonkon, "Structure, dissolution, and plant uptake of ferrous/zinc phosphates," *Chemosphere*, vol. 223, pp. 310-318, 2019.

[26] S. Li, S. Harris, A. Anandhi, and G. Chen, "Predicting biochar properties and functions based on feedstock and pyrolysis temperature: A review and data syntheses," *Journal of Cleaner Production*, vol. 215, pp. 890-902, 2019.

[27] N. Mojoudi, M. Soleimani, N. Mirghaffari, C. Belver, and J. Bedia, "Removal of phenol and phosphate from aqueous solutions using activated carbons prepared from oily sludge through physical and chemical activation," *Water Science and Technology*, vol. 80, pp. 575-586, 2019.

[28] Q. Yin, M. Liu, and H. Ren, "Removal of ammonium and phosphate from water by Mg-modified biochar: Influence of Mg pretreatment and pyrolysis temperature," *BioResources*, vol. 14, pp. 6203-6218, 2019.

[29] E. Wen, X. Yang, H. Chen, S. M. Shaheen, B. Sarkar, S. Xu, H. Song, Y. Liang, J. Rinklebe, D. Hou, Y. Li, F. Wu, M. Pohořelý, J. W. C. Wong, and H. Wang, "Iron-modified biochar and water management regime-induced changes in plant growth, enzyme activities, and phytoavailability of arsenic, cadmium and lead in a paddy soil," *Journal of Hazardous Materials*, vol. 407, p. 124344, 2021.

[30] J. Zhang, D. Hou, Z. Shen, F. Jin, D. O'Connor, S. Pan, Y. S. Ok, D. C. W. Tsang, N. S. Bolan, and D. S. Alessi, "Effects of excessive impregnation, magnesium content, and pyrolysis temperature on MgO-coated watermelon rind biochar and its lead removal capacity," *Environmental Research*, vol. 183, p. 109152, 2020.

[31] L. Wu, S. Zhang, J. Wang, and X. Ding, "Phosphorus retention using iron (II/III) modified biochar in saline-alkaline soils: Adsorption, column and field tests," *Environmental Pollution*, vol. 261, p. 114223, 2020.

[32] F. Zhang, X. Wang, J. Xionghui, and L. Ma, "Efficient arsenate removal by magnetite-modified water hyacinth biochar," *Environmental Pollution*, vol. 216, pp. 575-583, 2016.

[33] J. Bedia, M. Peñas-Garzón, A. Gómez-Avilés, J. J. Rodriguez, and C. Belver, "Review on activated carbons by chemical activation with $FeCl_3$," *C—Journal of Carbon Research*, vol. 6, p. 21, 2020.

[34] Z. Xu, T. Zhang, Z. Yuan, D. Zhang, Z. Sun, Y. Huang, W. Chen, D. Tian, H. Deng, and Y. Zhou, "Fabrication of cotton textile waste-based magnetic activated carbon using $FeCl_3$ activation by the Box–Behnken design: optimization and characteristics," *RSC Advances*, vol. 8, pp. 38081-38090, 2018.

[35] S. B. Kanungo, and S. K. Mishra, "Thermal dehydration and decomposition of $FeCl_3 \cdot xH_2O$," *Journal of Thermal Analysis*, vol. 46, pp. 1487-1500, 1996.

[36] H. Yang, R. Yan, H. Chen, D. H. Lee, and C. Zheng, "Characteristics of hemicellulose, cellulose and lignin pyrolysis," *Fuel*, vol. 86, pp. 1781-1788, 2007.

[37] A. C. Lua, and T. Yang, "Effect of activation temperature on the textural and chemical properties of potassium hydroxide activated carbon prepared from pistachio-nut shell," *Journal of Colloid and Interface Science*, vol. 274, pp. 594-601, 2004.

[38] R. R. Nair, M. M. Mondal, and D. Weichgrebe, "Biochar from co-pyrolysis of urban organic wastes—investigation of carbon sink potential using ATR-FTIR and TGA," *Biomass Conversion and Biorefinery*, 2020.

[39] Z. Shen, J. Zhang, D. Hou, D. C. W. Tsang, Y. S. Ok, and D. S. Alessi, "Synthesis of MgO-coated corncob biochar and its application in lead stabilization in a soil washing residue," *Environment International*, vol. 122, pp. 357-362, 2019.

[40] Z. Zhu, H. Zeng, Y. Zhu, F. Yang, H. Zhu, H. Qin, and W. Wei, "Kinetics and thermodynamic study of phosphate adsorption on the porous biomorph-genetic composite of α-Fe_2O_3/Fe_3O_4/C with eucalyptus wood microstructure," *Separation and Purification Technology*, vol. 117, pp. 124-130, 2013.

[41] J. H. Park, Y. S. Ok, S. H. Kim, J. S. Cho, J. S. Heo, R. D. Delaune, and D. C. Seo, "Evaluation of phosphorus adsorption capacity of sesame straw biochar on aqueous solution: influence of activation methods and pyrolysis temperatures," *Environmental Geochemistry and Health*, vol. 37, pp. 969-983, 2015.

[42] J. Qu, M. S. Akindolie, Y. Feng, Z. Jiang, G. Zhang, Q. Jiang, F. Deng, B. Cao, and Y. Zhang, "One-pot hydrothermal synthesis of $NaLa(CO_3)_2$ decorated magnetic biochar for efficient phosphate removal from water: Kinetics, isotherms, thermodynamics, mechanisms and reusability exploration," *Chemical Engineering Journal*, vol. 394, pp. 124915, 2020.

[43] R. Cai, X. Wang, X. Ji, B. Peng, C. Tan, and X. Huang, "Phosphate reclaim from simulated and real eutrophic water by magnetic biochar derived from water hyacinth," *Journal of Environmental Management*, vol. 187, pp. 212-219, 2017.

[44] M. Kosmulski, *Surface charging and points of zero charge*. Boca Raton: CRC Press, 2009.

[45] E. J. Elzinga, and D. L. Sparks, "Phosphate adsorption onto hematite: An in situ ATR-FTIR investigation of the effects of pH and loading level on the mode of phosphate surface complexation," *Journal of Colloid and Interface Science*, vol. 308, pp. 53-70, 2007.

[46] Y. Tu, Z. Peng, P. Xu, H. Lin, X. Wu, L. Yang, and J. Huang, "Characterization and application of magnetic biochars from corn stalk by pyrolysis and hydrothermal treatment," *BioResources*, vol. 12, pp. 1077-1089, 2016.

[47] J. F. Lustosa Filho, C. F. Barbosa, J. S. D. S. Carneiro, and L. C. A. Melo, "Diffusion and phosphorus solubility of biochar-based fertilizer: Visualization, chemical assessment and availability to plants," *Soil and Tillage Research*, vol. 194, p. 104298, 2019.

[48] M. B. Shakoor, S. Ali, M. Rizwan, F. Abbas, I. Bibi, M. Riaz, U. Khalil, N. K. Niazi, and J. Rinklebe, "A review of biochar-based sorbents for separation of heavy metals from water," *International Journal of Phytoremediation*, vol. 22, pp. 111-126, 2020.